First Scalable 18650 Aqueous-based Supercapacitors Using Hydrophobicity of Anti-corrosion Graphite Passivation Layer

Praeploy Chomkhuntod
Vidyasirimedhi Institute of Science and Technology
Pawin Iamprasertkun
Vidyasirimedhi Institute of Science and Technology https://orcid.org/0000-0001-7202-785X
Montree Sawangphruk (montree.s@vistec.ac.th)
Vidyasirimedhi Institute of Science and Technology

Article

Keywords:

Posted Date: November 30th, 2020

DOI: https://doi.org/10.21203/rs.3.rs-106698/v1

Abstract

Scalable 18650 aqueous-based supercapacitors are ideal as future energy storage technology due to their great safety, low cost, and environmental friendliness as well as high power density. Until now, there are no commercial aqueous-based supercapacitors due to the corrosion of metal current collectors. In this work, we have introduced a new concept using hydrophobicity of anti-corrosion graphite passivation layer coated on Al foil with high surface roughness leading to the lotus effect.

Main Text

The aqueous-based electrolytes for energy storage devices have been attractive due to their non-flammability along with non-toxicity.[1] Additionally, they provide higher power density (>10 kW kg^{-1}) than those using organic electrolytes,[2] ionic liquids,[3] and water-in-salt electrolytes due to the high ionic conductivity of aqueous solutions.[4,5] However, one of the key challenges limiting practical and commercial aqueous-based supercapacitors is a corrosion issue of metal current collectors in aqueous-based electrolytes. Recently, the surface modification of metals with carbon materials (i.e., graphite,[6,7] graphene,[8,9] and carbon nanotubes[10]) has attracted great attention for many other applications. Such reports highlighted remark improvements of the modified electrodes including the suppression of corrosion,[8] the improvement of interfacial contact,[9] and the reduction of internal resistance.[11] A graphite-coated aluminium current collector may be an ideal candidate to be coated on metal current collectors for the aqueous-based energy storage devices since the graphite is abundant providing great chemical stability and high electrical conductivity.[12] In addition, the fundamental investigation of graphite passivation layer on the current collector to the performance of energy storages is needed.

In this work, we have introduced an industrial roll-to-roll coating method of graphite with a finely tuned thickness of 25 μm on thin Al current collector with high surface roughness. It provides hydrophobicity, which is found in this work that it is a reason enhancing the anti-corrosion of the modified current collector. Interrestingly, we applied this concept to the first prototype of 18650-type cylindrical aqueous supercapacitors, which is the same size and shape as the commercial need.

Briefly, graphite slurry was coated firstly on the top and bottom layers of Al foil using a roll-to-roll coating process (see ESI†). The activated carbon, which is an active material of supercapacitors, was subsequently coated on the top layer of the first coated graphite layer. The specific surface area of activated carbon is ~2,158.85 $m^2 g^{-1}$ (see **Fig. S4a** and **Table S1** in ESI†), which is the same quality as the one used in the commercial supercapacitors with organic electrolytes.[13] The activated carbon was coated on the graphite coated Al foil (so-called “AC-GP”) and on the Al foil without graphite layer (so-called “AC-Al”) (see **Fig. 1**). Note, full experimental details can be found in ESI†. In **Fig. 1a**, the cross-sectional SEM image shows that the graphite was successfully coated on the Al surface with a thickness of *ca.* 25 μm finely tuned. The AC-GP shows strong interfacial contact between the active material layer and the modified current collector without air void (see **Fig. 1b**), while the AC-Al exhibits void spaces

between the material layer and the current collector (see **Fig. 1c**). This is a nature of materials for which a strong interfacial contact between carbon materials (graphite and activated carbon) can be observed. In addition, this suggests that the graphite protective layer can not only improve the interfacial contact but also enhance the charge transfer or reduce the internal resistance.[14] Apart from the morphologies, the time-dependence wettability of the modified substrate was also analysed using the Ossila Contact Angle in a high humidity chamber using a fixed droplet volume of 10 µL of the electrolyte (1 M Na_2SO_4) as shown in **Fig. 1d**. The graphite coated Al surface (AC-GP) exhibits the hydrophobic property with a contact angle (CA) of 93^o at t = 0.[15] Then, it is slghtly reduced to 90^o at t = 20 min. In contrast, the AC-Al demonstrates explicitly hydrophilic behaviour with a CA value of 80^o at t = 0, and reducing to 61^o at t = 20 min. This is due to the hydrophilic property of the thin film of native oxide (Al_2O_3) on the surface of Al foil.[16] It is clear that the graphite results in an increasing CA of the substrate, indicating that water is repelled from the Al surface. To confirm that the interfacial contact is involved in the electrochemical performance of the as-prepared electrodes, the cyclic voltammetry (CV) and galvanostatic charge-discharge (GCD) were evelauted using 1 M Na_2SO_4(aq) electrolyte in a three-electrode system at a potential range from -0.6 to 0.3 V vs. Hg/Hg_2SO_4. Note, details of the electrochemical cell setup and the procedure are given in ESI†.

The comparison of the CV profiles between the prepared electrodes with and without graphite layer at 10 mV s^{-1} (**Fig. 1e**) demonstrates that the current collector with the graphite layer shows a more rectangular CV shape and a significantly larger integrated area under the CV curve, corresponding to lower internal resistance and higher specific capacitance.[17] The AC-GP achieves a higher specific capacitance (105.3 F g^{-1}) than the AC-Al (42.1 F g^{-1}) at 10 mV s^{-1}. Moreover, the CV profile of AC-GP retains an almost rectangular shape with a capacitance of 77.6 F g^{-1} and a retention of 74% even at an increased scan rate of 100 mV s^{-1} (**Fig. S5a-b**, ESI†). This indicates a high level of electronic conductivity from good interfacial contact between the electrode material and the graphite-coated current collector.[18] Meanwhile, the AC-Al shows a significant distortion of the CV curves, indicating higher internal resistance.[17] This is due to the formation of more resistive oxide film and poor interfacial contact, leading to the low conductivity of the electrode.[17] As expected, the AC-Al shows rapid capacitance fading with much smaller retention, maintaining 18% at 100 mV s^{-1} (**Fig. S5c-d**, ESI†) due to the reasons discussed above. The electrochemical performance of graphite-coated Al foil was evaluated as a control, making clearer that the capacitance contribution from the graphite layer is negligible (only 1.06 mF g^{-1} at 10 mV s^{-1}) (see inset of **Fig. 1e).** Note that the surface area of the graphite is 8.46 m^2/g (see **Fig. S4b** and **Table S1** in ESI†).

Apart from the CV, the electrochemical performance was also investigated using GCD with respect to applied current densities. **Fig. 1f** shows that the AC-Al exhibits the smaller specific capacitance when compared with that of the AC-GP at the same current density. We can ascribe this to the formation of oxides on the Al foil surface during cycling, leading to the reduced capacitance.[14] The insets in **Fig. 1f** show the GCD profiles of AC-GP and AC-Al for which the GCD profiles of AC-GP exhibit a more

symmetrical triangular shape when compared with the AC-Al. This demonstrates that the coulombic efficiency of the AC-GP at 1 A g^{-1} is 84.2%, which is higher than 47.8% of the AC-Al, indicating the better electrochemical stability or reversibility.[19] In addition, the AC-GP shows a much smaller *iR* drop (25 mV) when compared to the AC-Al (199 mV) at 1 A g^{-1}, in which the *iR* drop corresponds to the internal resistance, indicating that the AC-Al has a higher resistance because of the formation of more Al_2O_3 resistive film on the Al foil surface.[20] This internal resistance leads to poor rate capability as shown in **Fig. 1f**, for which the AC-Al performs well only at very low current densities (from 0.5 to 3 A g^{-1}), with a dramatic fade in capacitance at 80% (from 29.2 to 6.8 F g^{-1}), leading to a lower power density. Conversely, the AC-GP shows outstanding rate capability with a slight capacitance fading – only 14% even at 20 A g^{-1} (87.7 F g^{-1}) as compared to 1 A g^{-1} (102.4 F g^{-1}), showing a strong capability for high rate charge/discharge, which represents the ideal behaviour for EDLCs.[21]

To further evaluate the passive oxide film on the Al foil, CV coupled with electrochemical impedance spectroscopy (EIS) was carried out on two different samples with and without the graphite coated layer. The results are shown in **Fig. 2**. The samples were subjected to 100 cycles at a scan rate of 100 mV s^{-1} and the EIS was then applied before cycling and after the 10^{th}, 25^{th}, 50^{th}, 75^{th}, and 100^{th} cycles. The CV profiles of the AC-GP maintain an almost rectangular shape even after the 100^{th} cycle (**Fig. 2a**), while the AC-Al shows a higher distortion with increased CV cycles (**Fig. 2b**), suggesting an increase in the internal resistance from the resistive oxide film grown on the Al foil during long cycling.[17] This can be more clearly observed from the Nyquist plots of the samples after cycling.

The EIS was evaluated at a voltage amplitude of 10 mV over the frequency range from 50 kHz to 0.01 Hz at an open-circuit potential (OCP) as shown in **Fig. 2c**. Overall, the charge transfer resistance (R_{CT}) is assigned to the contact resistance at the interface between the electrode material and the current collector, which can be evaluated from the semicircle in the Nyquist plot (inset **Fig. 2c**). The plot in **Fig. 2c** shows that the AC-GP electrode exhibits almost the same charge transfer resistance (about 0.4 Ω) after 100 cycles, which suggests that the interfacial properties of AC-GP remain unchanged after long cycling. In contrast, the R_{CT} of AC-Al significantly increases from 52.2 to 360.2 Ω after cycling as a result of the formation of a resistive oxide layer (Al_2O_3) as well as an increase in void spaces at the interface of the electrode after long cycling.[22,23]

In addition to the Nyquist plot, Bode phase diagrams were analysed (see **Fig. 3a-b**). It has been found that the electrode with a phase angle close to -90^o represents an ideal capacitor behaviour.[24] The AC-GP phase angles are closer to -90^o (**Fig. 3a**) when compared to the AC-Al (**Fig. 3b**), signifying the improved capacitive behaviour. Interestingly, the Bode diagrams of AC-GP and AC-Al show different profiles. While the AC-GP profiles display only EDLC behaviour (**Fig. 3a**), the AC-Al profiles show the characteristic peak of pseudocapacitive behaviour (**Fig. 3b**) because of the formation of the passive oxide film on the Al foil. More interestingly, the intensity of this peak increases after 100 cycles, indicating an increase in oxide film formation during cycling. The formation of the oxide film leads to poor capacitive behaviour, as

indicated by the change of phase angles of AC-Al from -68.6^{o} to -25.9^{o} after long cycling. The passive oxide film and the void space were further investigated by the *ex situ* characterisations. The *ex situ* SEM was carried out to confirm the void space generated after 100 cycles, which can clearly be observed in the cross-sectional images. The AC-GP shows an excellent level of the contact between the activated carbon layer and the graphite-modified Al foil even after 100 cycles (**Fig. 3c**), resulting in an excellent rate capability and a high level of stability. In contrast, the AC-Al exhibits a more detached active material layer from the Al surface (**Fig. 3d**) since the oxide film on the Al surface reduces the adhesion between the AC active material and the Al current collector.[25]

Moreover, the generated oxide film on the Al surface after long cycling can be further confirmed by the Al_2O_3 thin film as analysed by the *ex situ* XRD (see **Fig. 3e**). The ratio between Al_2O_3 and Al can be obtained from the XRD using the relative intensities of Al_2O_3 peak at 2θ=15.9^{o} (Al_2O_3 phase)[26] and Al peak at 2θ=38.2^{o} (111 plane).[27] The AC-Al shows a higher Al_2O_3 content of about 14.6% as compared with that of the AC-GP, indicating the graphite layer can reduce the Al_2O_3 film formation. Note, the Al_2O_3 film spontaneously grows on the Al foil surface at atmospereic condition having humidity. The characteristic peak of carbon shows a typical wide-angle XRD pattern at 22^{o} indicating the 002 plane of carbon, which represents the carbon materials.[28]

To further study the capacitive properties of those two samples, a complex capacitance model was applied according to **Eqn. S3-S4** (ESI†). In **Fig. S6a** (ESI†), Fast polarisation occurs in the high-frequency regions, presenting a resistor behaviour, while the capacitive behaviour is presented at lower frequencies due to the slower polarisation, resulting in the sufficient diffusion time of electrolytic ions. The transition region from the resistive to capacitive behaviours of the AC-GP moves to a higher frequency in comparison to the AC-Al, indicating that the AC-GP system can react to a faster changing polarisation due to the higher conductivity of the electrode.[29] Moreover, the kinetics of the electrode can be further described using the relaxation time constant (τ_0) in Bode plots of imaginary capacitances, where τ_0 refers to the minimum time required to discharge stored energy, which can be obtained from the peak frequency (see **Fig. S6b**, ESI†).[30] The τ_0 values of AC-GP and AC-Al are 3.30 and 6.19 s, respectively, indicating a faster charge/discharge capability for the AC-GP, which represents a higher rate of both capability and power density.

Fascinatingly, we have successfully fabricated the first prototype of an 18650 cell type supercapacitor in an aqueous electrolyte system using 1 M Na_2SO_4. The charge storage performance was investigated using the GCD method from 50 mA to 1000 mA as shown in **Fig. 4a** and **Fig. S7** (ESI†). As expected, the AC-GP in **Fig. 4a** shows a higher cell capacitance (18.9 F) than the AC-Al (13.1 F at 50 mA) as well as the AC-GP exhibits a lower *iR* drop (13 mV) than that of AC-Al (85.6 mV) (see inset of **Fig. 4a**), indicating a better electrical conductivity in the electrode.[31] Moreover, the AC-GP electrode shows an excellent maintenance rate capability with remained at 82.4% even at 1000 mA (15.6 F). Unlike the AC-GP, the AC-Al can perform at currents of less than 250 mA and the capacitance retention is reduced 17.2% when the current is increased from 50 to 250 mA. Moreover, the stability of the assembled devices was further

evaluated at 100 mA/cell. **Fig. 4b** shows that the AC-GP is maintained at almost 100% of capacitance after 3,000 cycles. In contrast, the AC-Al exhibits a rapid capacitance fade, and only 19.4% of its capacitance is maintained because of the corrosion of the Al foil (the formation of oxides) as well as an increase in void space over long cycling. The assembled devices were further investigated in terms of their internal resistance by following the IEC 62391-1 standard (**Fig. S8**, ESI†). The internal resistance was described in terms of the equivalent series resistance (ESR), and the ESR of AC-GP shows a smaller resistance (0.2 Ω) than the AC-Al (0.6 Ω) which leads to a higher conductivity rate in the electrode, resulting in a higher power delivery of the device.[32]

This transition region is shifted to a higher frequency, if the system can react to the changing polarization, that is, the better the ions can diffuse within the material. This transition region is shifted to a higher frequency, if the system can react to the changing polarization, that is, the better the ions can diffuse within the material.

In summary, a graphite coating was successfully fabricated on the Al foil addressing its corrosion issue in aqueous-based electrolytes. The graphite layer improves the adhesion between the active material layer and the current collector as well as helps to preserve the surface of the Al foil, preventing the formation of a passive oxide film (Al_2O_3). It also accelerates the charge transfer and reduces the internal resistance. The electrode with the graphite layer (AC-GP) demonstrates a higher specific capacitance (105.3 F g^{-1}) than that of AC-Al (42.1 F g^{-1}) at 10 mV s^{-1} as well as higher stability. The 18650 prototype of supercapacitors proves that the finding of this study should lead to practical aqueous supercapacitors with great safety and power density.

Declarations

Conflicts of interest

There are no conflicts to declare.

References

1 Xiong, T., Tan, T. L., Lu, L., Lee, W. S. V. & Xue, J. Harmonizing Energy and Power Density toward 2.7 V Asymmetric Aqueous Supercapacitor. *Adv. Energy Mater.* **8**, 1702630, doi:10.1002/aenm.201702630 (2018).

2 Wang, W. *et al.* A hybrid superconcentrated electrolyte enables 2.5 V carbon-based supercapacitors. *Chem. Commun.* **56**, 7965-7968, doi:10.1039/D0CC02040K (2020).

3 Zhong, H., Xu, F., Li, Z., Fu, R. & Wu, D. High-energy supercapacitors based on hierarchical porous carbon with an ultrahigh ion-accessible surface area in ionic liquid electrolytes. *Nanoscale* **5**, 4678-4682, doi:10.1039/C3NR00738C (2013).

4 Iamprasertkun, P., Ejigu, A. & Dryfe, R. A. W. Understanding the electrochemistry of “water-in-salt” electrolytes: basal plane highly ordered pyrolytic graphite as a model system. *Chem. Sci.* **11**, 6978-6989, doi:10.1039/D0SC01754J (2020).

5 Wang, C. *et al.* Polyaniline functionalized reduced graphene oxide/carbon nanotube ternary nanocomposite as a supercapacitor electrode. *Chem. Commun.* **56**, 4003-4006, doi:10.1039/D0CC01028F (2020).

6 Arvani, M., Keskinen, J., Lupo, D. & Honkanen, M. Current collectors for low resistance aqueous flexible printed supercapacitors. *J. Energy Storage* **29**, 101384, doi:https://doi.org/10.1016/j.est.2020.101384 (2020).

7 Sahoo, B., Kumar, R., Joseph, J., Sharma, A. & Paul, J. Preparation of aluminium 6063-graphite surface composites by an electrical resistance heat assisted pressing technique. *Surf. Coat. Technol.* **309**, 563-572, doi:https://doi.org/10.1016/j.surfcoat.2016.12.011 (2017).

8 Li, X. *et al.* Suppressing Corrosion of Aluminum Foils via Highly Conductive Graphene-like Carbon Coating in High-Performance Lithium-Based Batteries. *ACS Appl. Mater. Interfaces* **11**, 32826-32832, doi:10.1021/acsami.9b06442 (2019).

9 Kim, S. Y. *et al.* Few-layer graphene coated current collectors for safe and powerful lithium ion batteries. *Carbon* **153**, 495-503, doi:https://doi.org/10.1016/j.carbon.2019.07.032 (2019).

10 Yao, Y. *et al.* Epitaxial Welding of Carbon Nanotube Networks for Aqueous Battery Current Collectors. *ACS Nano* **12**, 5266-5273, doi:10.1021/acsnano.7b08584 (2018).

11 Wang, R. *et al.* Carbon black/graphene-modified aluminum foil cathode current collectors for lithium ion batteries with enhanced electrochemical performances. *J. Electroanal. Chem.* **833**, 63-69, doi:https://doi.org/10.1016/j.jelechem.2018.11.007 (2019).

12 Hu, H. *et al.* Small graphite nanoflakes as an advanced cathode material for aluminum ion batteries. *Chem. Commun.* **56**, 1593-1596, doi:10.1039/C9CC06895C (2020).

13 Li, B. *et al.* Nitrogen-doped activated carbon for a high energy hybrid supercapacitor. *Energy Environ. Sci.* **9**, 102-106, doi:10.1039/C5EE03149D (2016).

14 Kuenzel, M. *et al.* Unveiling and Amplifying the Benefits of Carbon-Coated Aluminum Current Collectors for Sustainable LiNi0.5Mn1.5O4 Cathodes. *ACS Appl. Energy Mater.* **3**, 218-230, doi:10.1021/acsaem.9b01302 (2020).

15 Wei, Y. & Jia, C. Q. Intrinsic wettability of graphitic carbon. *Carbon* **87**, 10-17, doi:https://doi.org/10.1016/j.carbon.2015.02.019 (2015).

16 Nakajima, D. *et al.* A Superhydrophilic Aluminum Surface with Fast Water Evaporation Based on Anodic Alumina Bundle Structures via Anodizing in Pyrophosphoric Acid. *Materials* **12**, 3497 (2019).

17 Bu, X., Su, L., Dou, Q., Lei, S. & Yan, X. A low-cost “water-in-salt” electrolyte for a 2.3 V high-rate carbon-based supercapacitor. *J. Mater. Chem. A* **7**, 7541-7547, doi:10.1039/C9TA00154A (2019).

18 Peng, H. *et al.* Pore and Heteroatom Engineered Carbon Foams for Supercapacitors. *Adv. Energy Mater.* **9**, 1803665, doi:10.1002/aenm.201803665 (2019).

19 Wu, F. *et al.* Hierarchical porous carbon microrods derived from albizia flowers for high performance supercapacitors. *Carbon* **147**, 242-251, doi:https://doi.org/10.1016/j.carbon.2019.02.072 (2019).

20 Wang, D. *et al.* Unconventional mesopore carbon nanomesh prepared through explosion–assisted activation approach: A robust electrode material for ultrafast organic electrolyte supercapacitors. *Carbon* **119**, 30-39, doi:https://doi.org/10.1016/j.carbon.2017.03.102 (2017).

21 Yang, M. *et al.* Fabrication of High-Power Li-Ion Hybrid Supercapacitors by Enhancing the Exterior Surface Charge Storage. *Adv. Energy Mater.* **5**, 1500550, doi:10.1002/aenm.201500550 (2015).

22 Mei, B.-A., Munteshari, O., Lau, J., Dunn, B. & Pilon, L. Physical Interpretations of Nyquist Plots for EDLC Electrodes and Devices. *J. Phys. Chem. C* **122**, 194-206, doi:10.1021/acs.jpcc.7b10582 (2018).

23 Rosliza, R., Wan Nik, W. B., Izman, S. & Prawoto, Y. Anti-corrosive properties of natural honey on Al–Mg–Si alloy in seawater. *Curr. Appl. Phys.* **10**, 923-929, doi:https://doi.org/10.1016/j.cap.2009.11.074 (2010).

24 Yang, W. *et al.* Supercapacitance of nitrogen-sulfur-oxygen co-doped 3D hierarchical porous carbon in aqueous and organic electrolyte. *J. Power Sources* **359**, 556-567, doi:https://doi.org/10.1016/j.jpowsour.2017.05.108 (2017).

25 Wojciechowski, J., Kolanowski, Ł., Bund, A. & Lota, G. The influence of current collector corrosion on the performance of electrochemical capacitors. *J. Power Sources* **368**, 18-29, doi:https://doi.org/10.1016/j.jpowsour.2017.09.069 (2017).

26 Gangwar, J., Gupta, B. K., Kumar, P., Tripathi, S. K. & Srivastava, A. K. Time-resolved and photoluminescence spectroscopy of θ-Al2O3 nanowires for promising fast optical sensor applications. *Dalton Trans.* **43**, 17034-17043, doi:10.1039/C4DT01831A (2014).

27 Aliyu, I. K., Saheb, N., Hassan, S. F. & Al-Aqeeli, N. Microstructure and Properties of Spark Plasma Sintered Aluminum Containing 1 wt.% SiC Nanoparticles. *Metals* **5**, 70-83 (2015).

28 Atchudan, R., Edison, T. N. J. I., Perumal, S. & Lee, Y. R. Green synthesis of nitrogen-doped graphitic carbon sheets with use of Prunus persica for supercapacitor applications. *Appl. Surf. Sci.* **393**, 276-286,

doi:https://doi.org/10.1016/j.apsusc.2016.10.030 (2017).

29 Borchardt, L., Leistenschneider, D., Haase, J. & Dvoyashkin, M. Revising the Concept of Pore Hierarchy for Ionic Transport in Carbon Materials for Supercapacitors. *Adv. Energy Mater.* **8**, 1800892, doi:10.1002/aenm.201800892 (2018).

30 Yu, J. *et al.* Ultrahigh-rate wire-shaped supercapacitor based on graphene fiber. *Carbon* **119**, 332-338, doi:https://doi.org/10.1016/j.carbon.2017.04.052 (2017).

31 Wang, S. *et al.* N-doped carbon spheres with hierarchical micropore-nanosheet networks for high performance supercapacitors. *Chem. Commun.* **50**, 12091-12094, doi:10.1039/C4CC04832F (2014).

32 Kim, B.K., et al. Electrochemical Supercapacitors for Energy Storage and Conversion in *Handbook of Clean Energy Systems*1-25 (2015) doi/10.1002/9781118991978.hces112.

Figures

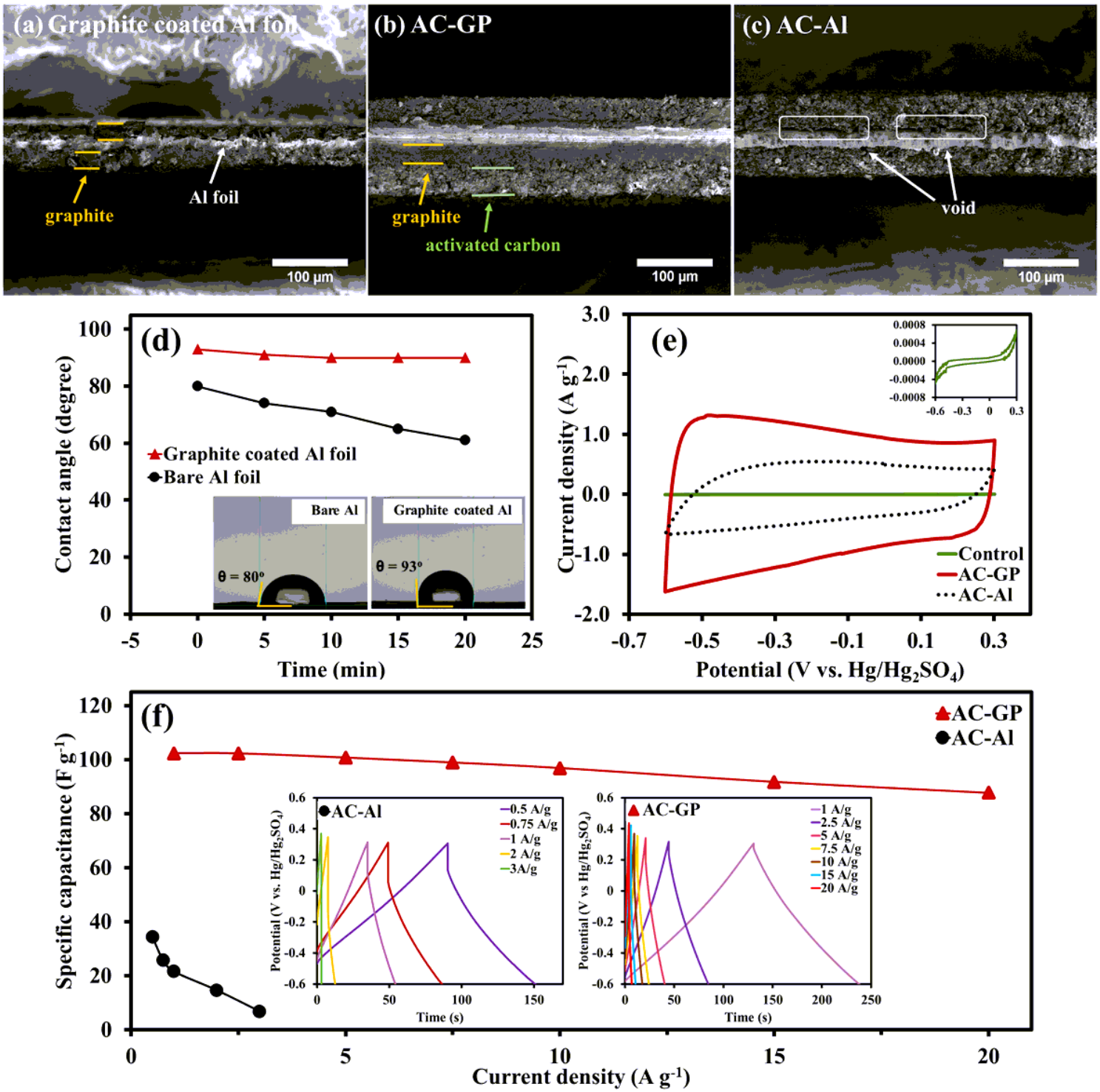

Figure 1

SEM images of (a) graphite coated Al foil, (b) AC-GP, and (c) AC-Al; (d) CA vs. immersion time (inset: the drops of 1 M Na2SO4 at t = 0 min); (e) CVs at 10 mV s-1 (inset: CV profile of a control); and (f) specific capacitances as a function of current densities (inset: GCD profiles at various current densities).

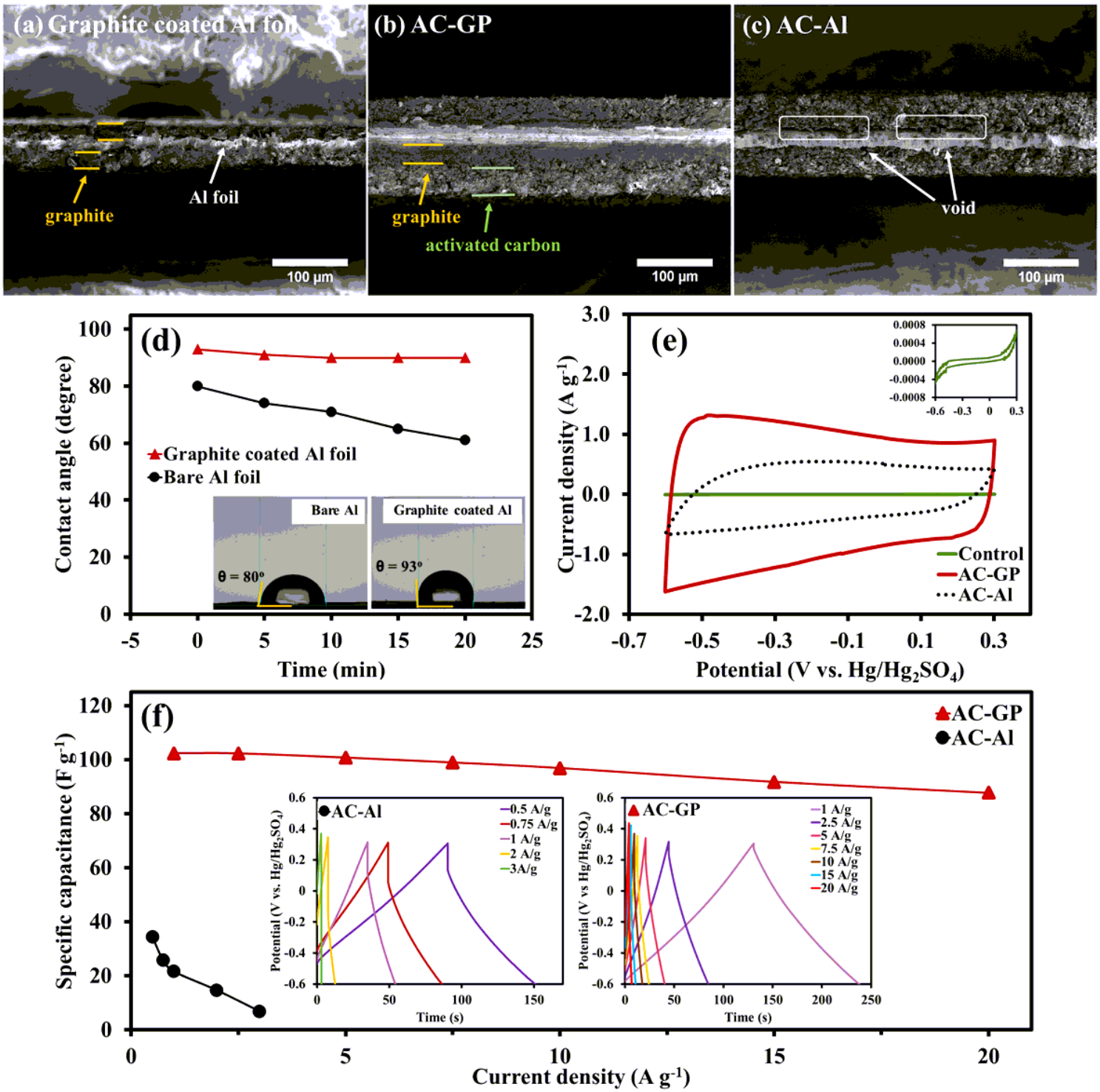

Figure 1

SEM images of (a) graphite coated Al foil, (b) AC-GP, and (c) AC-Al; (d) CA vs. immersion time (inset: the drops of 1 M Na2SO4 at t = 0 min); (e) CVs at 10 mV s-1 (inset: CV profile of a control); and (f) specific capacitances as a function of current densities (inset: GCD profiles at various current densities).

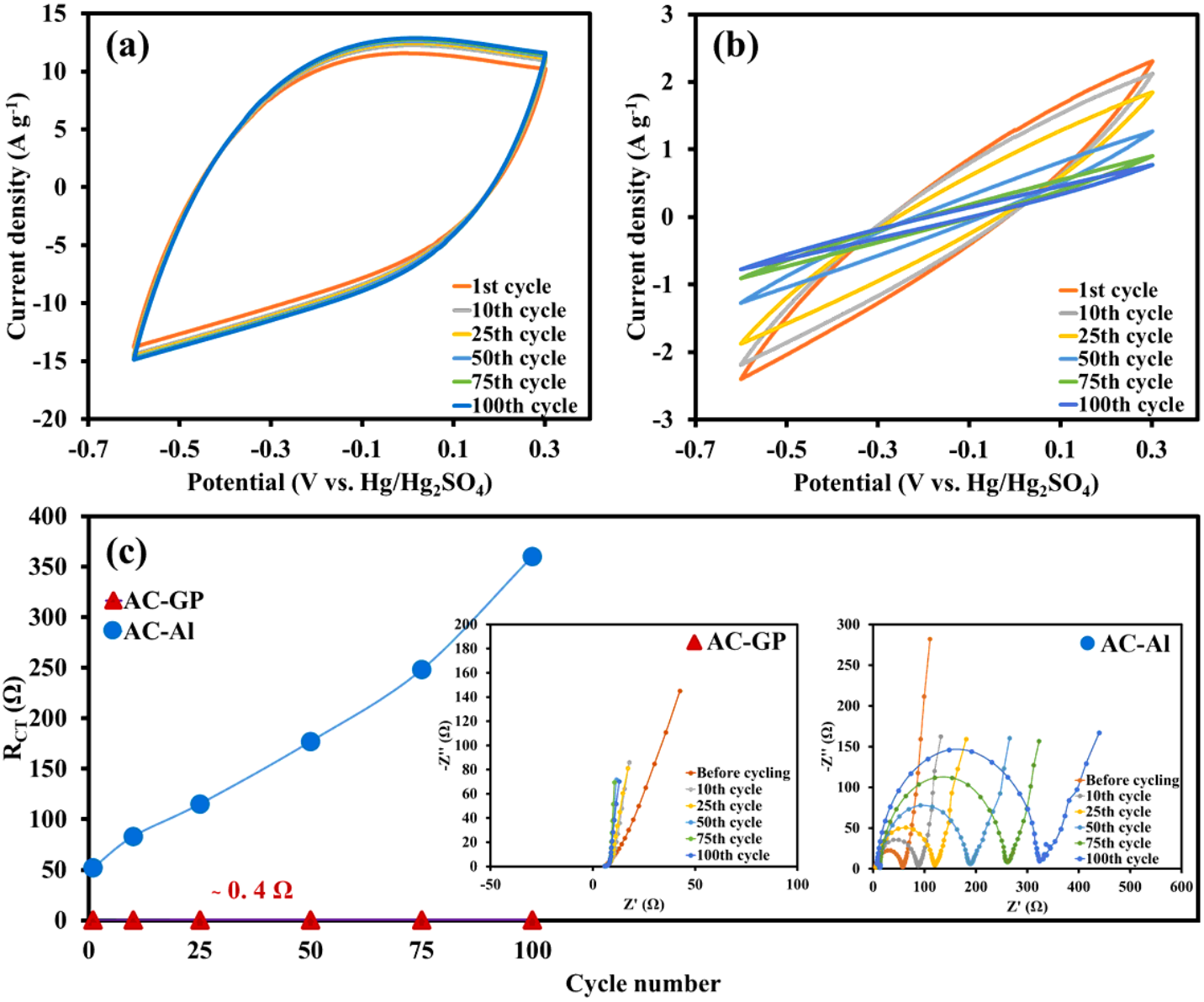

Figure 2

2 CVs at 100 mV s-1 of (a) AC-GP and (b) AC-Al and (c) Summarised RCT values as a function of cycle numbers (inset: Nyquist plots).

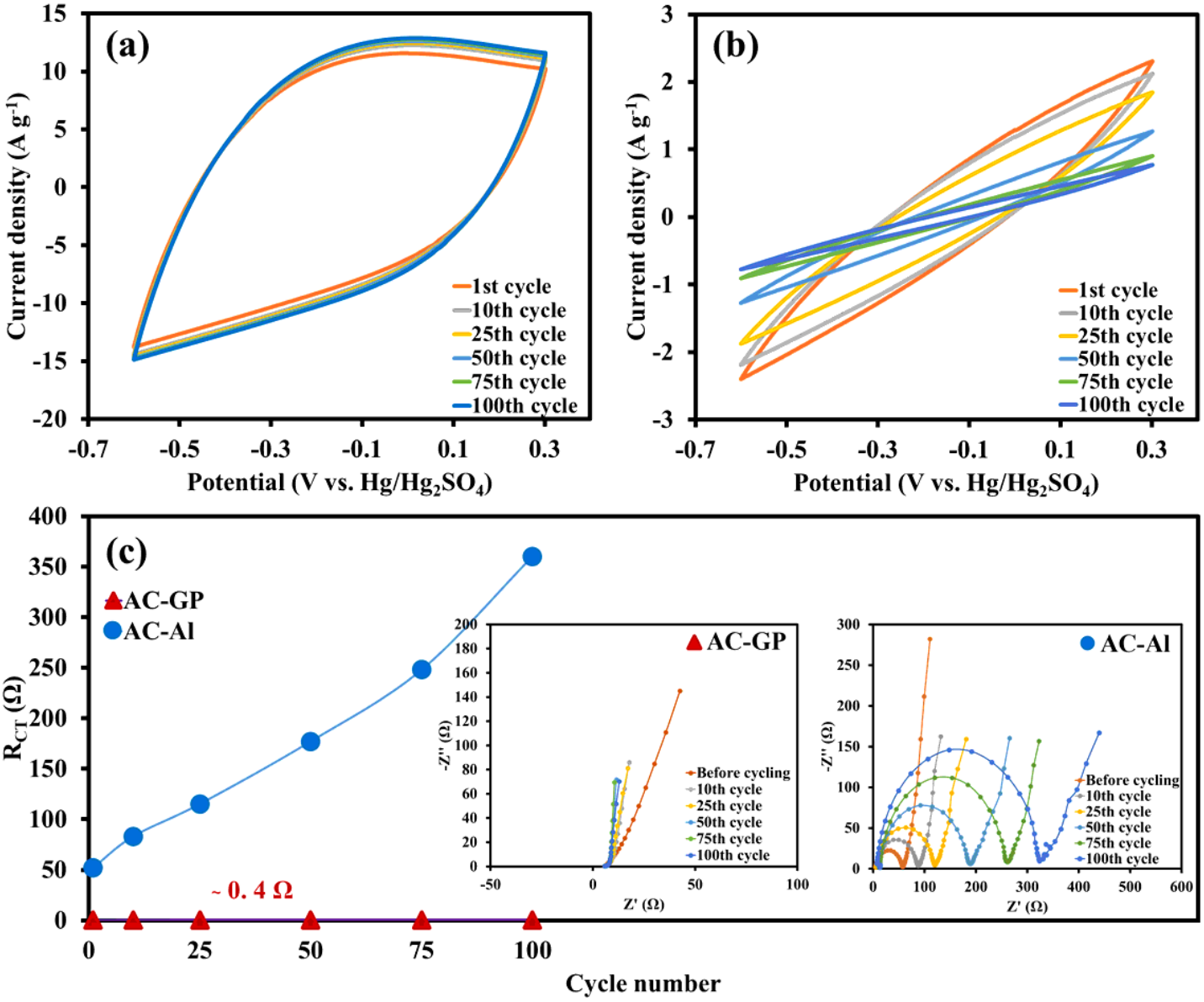

Figure 2

2 CVs at 100 mV s-1 of (a) AC-GP and (b) AC-Al and (c) Summarised RCT values as a function of cycle numbers (inset: Nyquist plots).

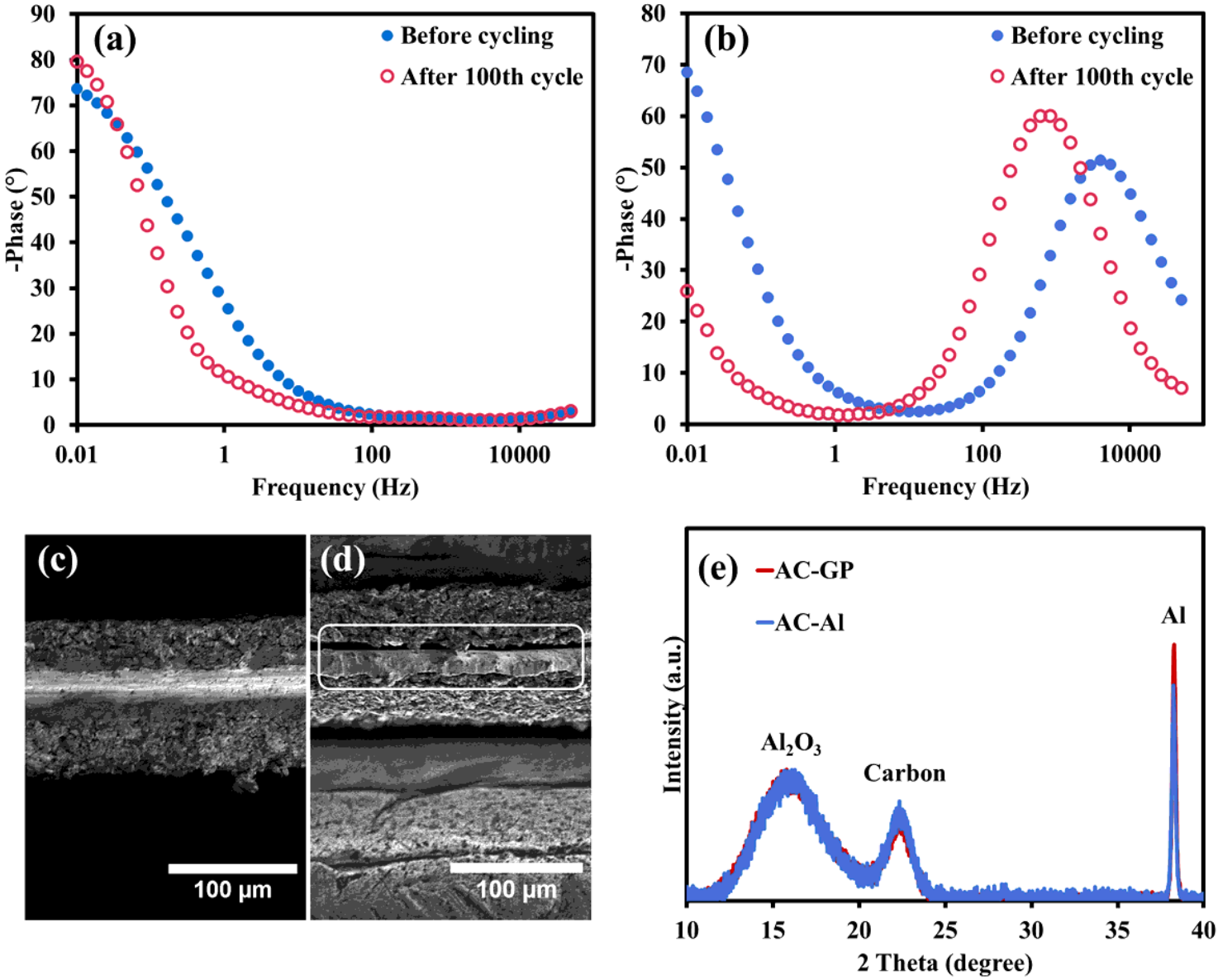

Figure 3

Bode phase diagrams of (a) AC-GP and (b) AC-Al and ex situ cross-sectional SEM images of (c) AC-GP and (d) AC-Al images after the 100th cycle via CV, and (e) ex situ XRD patterns of Al2O3 thin film compared with Al of the as-prepared electrodes after cycling for 100 cycles.

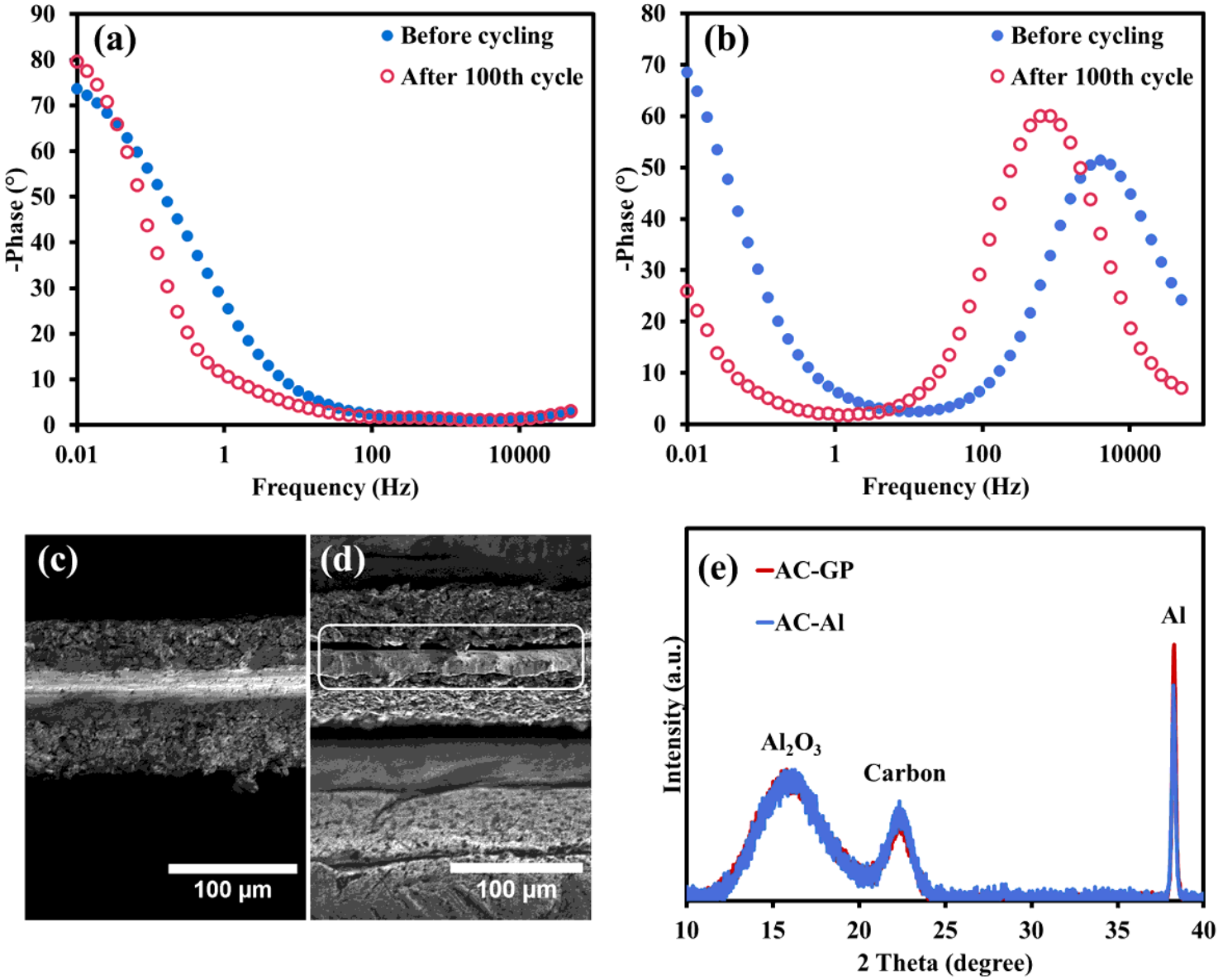

Figure 3

Bode phase diagrams of (a) AC-GP and (b) AC-Al and ex situ cross-sectional SEM images of (c) AC-GP and (d) AC-Al images after the 100th cycle via CV, and (e) ex situ XRD patterns of Al2O3 thin film compared with Al of the as-prepared electrodes after cycling for 100 cycles.

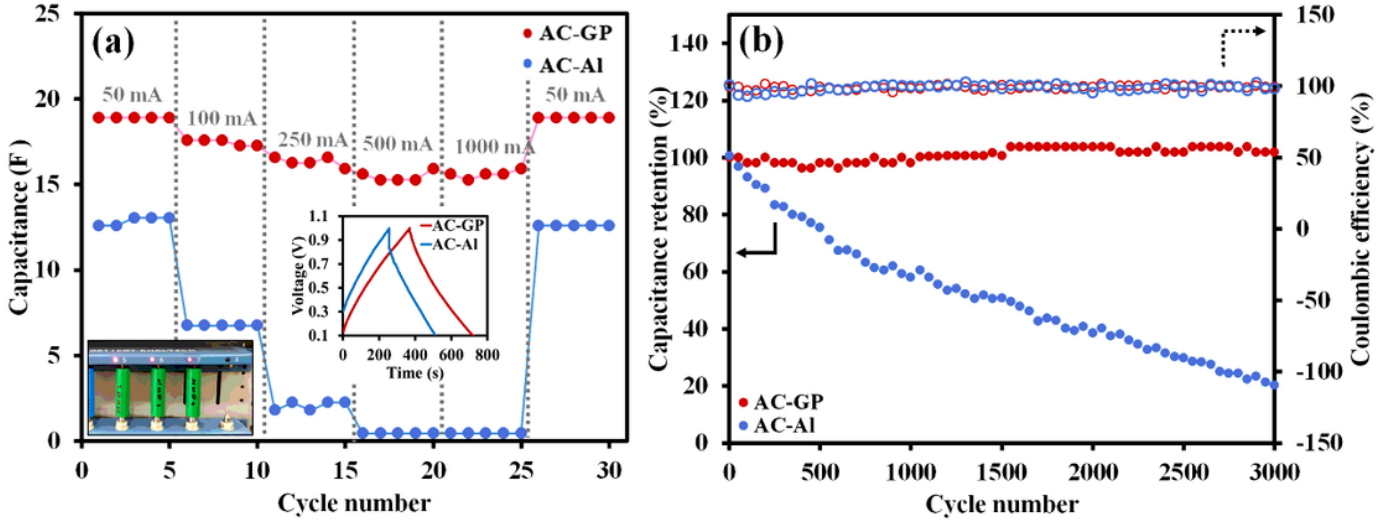

Figure 4

(a) Rate capability of the 18650 cylindrical cells of AC-GP and AC-Al, and (b) stability at 100 mA.

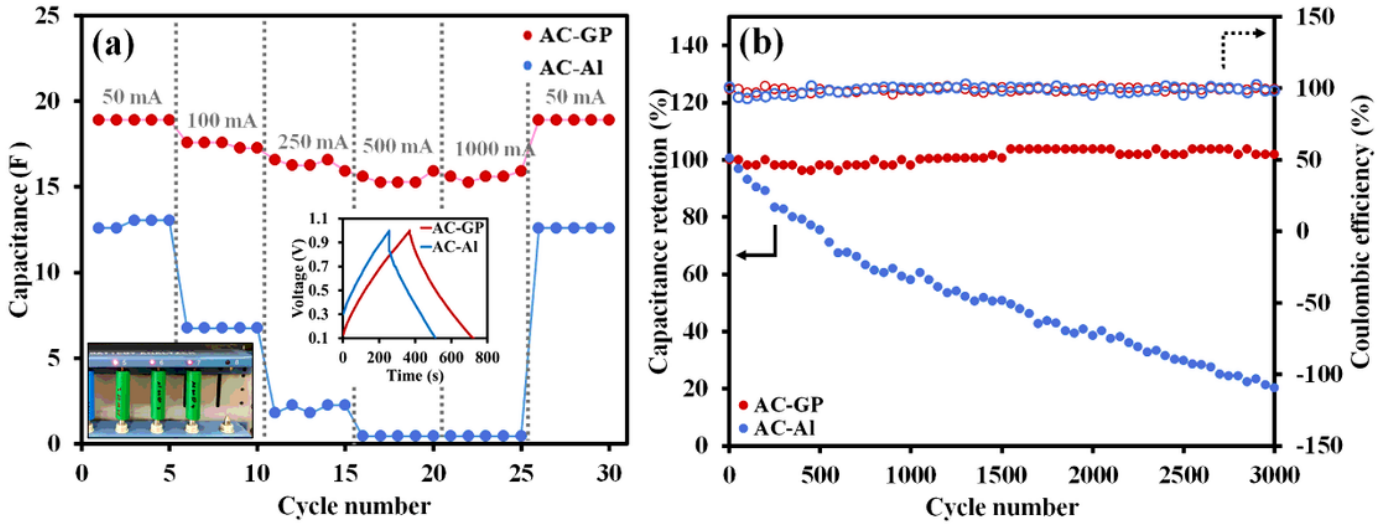

Figure 4

(a) Rate capability of the 18650 cylindrical cells of AC-GP and AC-Al, and (b) stability at 100 mA.

Supplementary Files

This is a list of supplementary files associated with this preprint. Click to download.

- SI12112020.docx
- SI12112020.docx